Eur. Phys. J. E (2013) **36**: 113
DOI 10.1140/epje/i2013-13113-1

THE EUROPEAN PHYSICAL JOURNAL E

Regular Article

Acoustic characterisation of liquid foams with an impedance tube

Juliette Pierre[1], Reine-Marie Guillermic[2], Florence Elias[1,3], Wiebke Drenckhan[2], and Valentin Leroy[1,a]

[1] Laboratoire MSC, Université Paris-Diderot, CNRS (UMR 7057), Paris, France
[2] Laboratoire de Physique des Solides, Université Paris-Sud - UMR 8502, Orsay, France
[3] Université Pierre et Marie Curie, 4 place Jussieu, 75252 Paris Cedex 05, France

Received 19 April 2013 and Received in final form 24 July 2013
Published online: 15 October 2013 –

Abstract. Acoustic measurements provide convenient non-invasive means for the characterisation of materials. We show here for the first time how a commercial impedance tube can be used to provide accurate measurements of the velocity and attenuation of acoustic waves in *liquid* foams, as well as their effective "acoustic" density, over the 0.5–6 kHz frequency range. We demonstrate this using two types of liquid foams: a commercial shaving foam and "home-made" foams with well-controlled physico-chemical and structural properties. The sound velocity in the latter foams is found to be independent of the bubble size distribution and is very well described by Wood's law. This implies that the impedance technique may be a convenient way to measure *in situ* the density of liquid foams. Important questions remain concerning the acoustic attenuation, which is found to be influenced in a currently unpredictible manner by the physico-chemical composition and the bubble size distribution of the characterised foams. We confirm differences in sound velocities in the two types of foams (having the same structural properties) which suggests that the physico-chemical composition of liquid foams has a non-negligible effect on their acoustic properties.

1 Introduction

Liquid foams consist of closely packed gas bubbles, which are immersed in a liquid carrier matrix and stabilised by surfactants [1,2]. They are widely used in applications and as model systems to deepen our understanding of the physical properties of complex fluids. Due to their complex properties, *in situ* characterisation of structural or dynamic properties of liquid foams remains a great challenge. This concerns in particular their acoustic properties. Whilst acoustic characterisation has become a standard technique in the case of solid foams [3], emulsions or particulate dispersions [4], the acoustic properties of liquid foams remain to be elucidated. Isolated progress has been made in the subject [5,6], showing, for example that the isothermal Wood's law [7] may be used reliably to predict the velocity of sound in most liquid foams, when the bubbles are much smaller than the acoustic wavelength

$$v_W = \sqrt{P_0/(\rho_\ell \Phi(1-\Phi))}, \qquad (1)$$

where P_0 is the ambient pressure, ρ_ℓ the mass density of the liquid and Φ the liquid volume fraction. However, for some foams [8,9], the sound velocity is larger than what is predicted by Wood's law. Of particular interest is the presence of resonance effects [10–12]. This may provide an elegant tool for bubble size measurements in liquid foams, but its precise nature remains to be elucidated. Furthermore, many questions remain concerning the complex interplay of different dissipation mechanisms and the influence of the physico-chemical nature of the foam. For example, it is not clear how the presence of an interfacial or bulk visco-elasticity influences the acoustic properties of the foam.

Comparison of acoustic investigations done up to date remains a challenging exercise due to significant variations in acoustic techniques applied or types of foams used (see appendix B). To overcome this problem, we propose here the use of a well-established, commercially available tool: the impedance tube [13]. This technique is widely used for the characterisation of porous media for frequencies up to a few kilohertz. It is usually not used with liquids, but we show here that the same device can be employed for the characterisation of liquid foams without technical adaptation (sect. 2.3). We furthermore propose a procedure for analyzing the data to obtain precise measurements of the foam density, and velocity and attenuation of the acoustic waves for a frequency range of 0.5–6 kHz (sect. 3). We demonstrate the success of this approach (sect. 4) using liquid foams in which we control explicitely the most important parameters, such as the physico-chemical composition, the bubble size distribution and the liquid volume fraction (sect. 2.2). We show

[a] e-mail: valentin.leroy@univ-paris-diderot.fr

that care needs to be taken when working with physico-chemically less controlled foams like shaving foams, as has been done in the past.

The interest of the application of this impedance technique to liquid foams is two-fold. On the one hand, it may provide a convenient tool for the *in situ* characterisation of liquid foams. On the other hand, it may help shedding light on important questions concerning the response of liquid foams to rapid deformations in complementing more established foam characterisation techniques (like rheometers), which are limited to excitation frequencies of about 10 Hz.

2 Materials and methods

2.1 Materials

The samples investigated here are liquid foams. We chose two representative systems. The first one is a commercial shaving foam (Gillette, "Sensitive skin") which serves to compare with previous literature [9,11,14]. The bubbles of a shaving foam are composed of mixtures of butane/propane and the foaming solution contains a complex physico-chemical composition designed to optimise the stability and flow properties of the foam. Since this exact composition is unknown, we have chosen to work in parallel with a physico-chemically simpler system whose composition we can control. For this purpose we use an aqueous solution (millipore water) containing 10 g/L of SDS (sodium dodecyl sulfate) and 0.5 g/L of xanthane. SDS is known to be a good foamer, while xanthane is an anionic polysaccharide (Sigma Aldrich) with a cellulosic backbone which is commonly used as foam stabiliser [15]. This is due to its visco-elastic nature even at low concentration, which slows down the gravity-driven drainage of liquid between the bubbles (appendix C). Moreover, xanthane solutions are strongly shear thinning at the concentrations used here, which is an important prerequisit for reliable foaming. In order to further reduce any ageing effects of the foam, we generate the foams using air containing C_6F_{14}, which is nearly insoluble in water. The presence of these molecules generates strong partial pressures which conteract the typically encountered exchange of more soluble gasses (like nitrogen in air) between bubbles of different pressures. Combining the effect of the xanthane and the C_6F_{14}, we can reasonably assume that the foams remain homogeneous during the acoustic measurement (less than 1 min). Only in the case of foams containing a high liquid content, the effect of the xanthane is less efficient, hence leading to a gradient in liquid fraction, which is discussed in more detail in appendix C. Note that Gillette foams are also known for ageing very slowly [11].

2.2 Foaming and foam characterisation

Gillette foams are generated by simply dispensing them from their commercial foaming device. In order to generate SDS foams with similar bubbles sizes and liquid fractions,

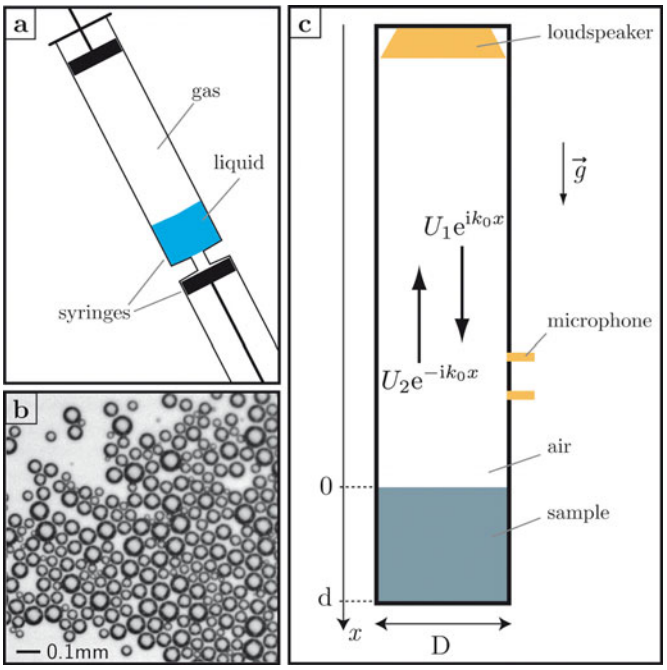

Fig. 1. Scheme of the setups used to produce (a), characterise (b) and measure the acoustical properties (c) of liquid foams. (a) With the two-syringe technique, liquid foams with tens of micrometers bubbles and controlled liquid fraction can be obtained. (b) Typical image of a bubble raft analysed for bubble size determination (here sample SDS 5% A). (c) Impedance tube: the reflection coefficient $\mathcal{R} = U_2/U_1$ of the sample is determined by measuring the pressure field with two wall-mounted microphones. Note that for measurements with liquid foams, the tube is hold vertically.

we use a double-syringe technique (see fig. 1a). This technique consists in connecting two syringes which contain the gas and the liquid to be foamed. By repeatedly pushing liquid and gas from one syringe to the other through the narrow connection (here 10 mm long and 1.6 mm wide), both mix due to the strong shearing action in the constriction and create a homogenous foam with bubble sizes of the order of 10–100 micrometers. The liquid fraction of the final foam is fixed by the ratio of the amount of liquid to the total internal volume of one syringe. If the liquid phase has a good foamability, liquid fractions from 3 to 30% can be obtained, with a typical accuracy of 1% with the syringes we used.

In order to measure the bubble size distribution of the different generated foams, we take a small drop of the liquid foam and pour it on a bath of the foaming liquid, hence generating a monolayer of bubbles (see fig. 1b). This two-dimensional structure can be easily imaged using a digital camera and analysed using an image analysis software (see appendix A). We show two typical size distributions in fig. 2, for a Gillette and an SDS foam. We use these distributions to calculate the mean bubble radius, the polydisperse index (normalised standard deviation) and the Sauter mean radius ($R_{32} = \langle R^3\rangle/\langle R^2\rangle$) [16], the latter of which is commonly the more appropriate quantity in the description of dynamic properties of polydisperse foams

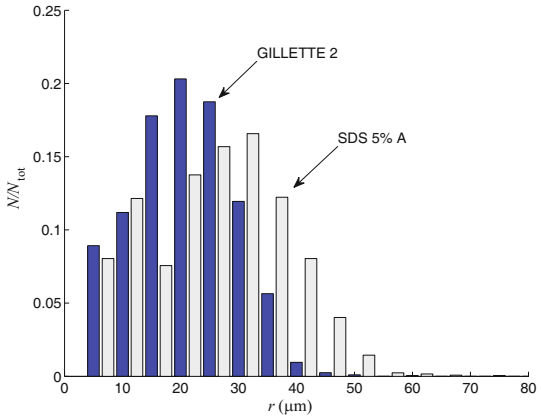

Fig. 2. Histograms of two representative bubble size distributions, for two liquid foam samples.

Table 1. Liquid fraction Φ, mean bubble radius $\langle R\rangle$, polydispersity index PI and Sauter mean radius R_{32} for 8 of the investigated liquid foams. The liquid fractions reported for the SDS samples correspond to the target value of the 2-syringe technique; for the Gillette samples, Φ was estimated by weighting.

Sample	Φ (%)	$\langle R\rangle$ (μm)	PI	R_{32} (μm)
SDS 5% A	5	27	0.42	38
SDS 5% B	5	54	0.65	120
SDS 10% A	10	22	0.46	33
SDS 10% B	10	20	0.70	53
SDS 20% A	20	16	0.49	26
SDS 20% B	20	25	0.57	46
GILLETTE 1	7	26	0.51	44
GILLETTE 2	7	22	0.43	32

since it measures the volume to surface ratio of the bubbles.

The results of sect. 4 will be discussed using eight representative foam samples whose properties are summarised in table 1. It is important to note that the difference between the A and the B SDS foams resides in the content of C_6F_{14} in the gas of the bubbles. While in the A group the air had been saturated with C_6F_{14}, foams of the B group have a very small amount of C_6F_{14}.

2.3 Acoustic measurements

The acoustic measurements were performed with a commercial impedance tube (type 4206, B&K), which employs the two-microphone technique [17,13,18]. The principle of the method is the following: a loudpseaker generates plane waves in the tube, which are reflected by the sample with a reflection coefficient $\mathcal{R} = U_2/U_1$ (see fig. 1c). By measuring the pressure field at two points in the tube, one can determine $\mathcal{R}$, which is related to the acoustic impedance of the sample. As shown in sect. 3, if the thickness d of the sample is precisely known, one can determine the density of the sample, as well as the acoustic velocity and attenuation.

In practice, the impedance tube was installed vertically and the liquid foam was poured into the sample holder, typically on a thickness of the order of 2 cm. Then its surface was flattened and, if necessary, the position of the backwall was adapted so that the surface of the liquid foam was at $x_0 = 0$ (see appendix D). The tube was closed with the sample in place, and the acoustic measurement was performed, which took less than one minute. After the measurement, the holder was opened and the precise thickness of the sample was measured with a caliper (± 0.5 mm). Bubble sizes were measured before and after the acoustic measurement and found to be the same.

Due to gravity, there is a gradient of liquid fraction within the foam. However, given the bubble sizes and the thickness investigated here, the samples can be considered as homogeneous to a first approximation. Indeed, a characteristic length over which the foam may be considered as homogenous can be estimated by $\ell_c^2/(\sqrt{\Phi}R_{32})$ [19], where $\ell_c = \sqrt{\gamma/\rho g}$ is the capillary length. This is of the order of 20 cm for most of the foams we consider (see table 1). A more detailed discussion of the drainage can be found in appendix C.

3 Data analysis

In the case of a semi-infinite sample, the reflection coefficient is directly related to the impedance Z of the sample by $\mathcal{R} = (Z - Z_0)/(Z + Z_0)$, where Z_0 is the impedance of air[1]. In the case of a finite sample, one defines an *input* impedance $Z^\star$ (also known as the surface impedance), which accounts for the multiple reflections in the sample, defined by

$$Z_0/Z^\star = \frac{1-\mathcal{R}}{1+\mathcal{R}}\,. \tag{2}$$

$Z_0/Z^\star$ is the dimensionless input admittance of the sample. The backplate behind the sample (at $x = d$) being designed to be perfectly rigid, the input impedance is given by

$$Z^\star = \mathrm{i}Z/\tan(kd), \tag{3}$$

where $k = k' + \mathrm{i}k''$ is the complex wave number in the sample, and d its thickness. As $Z = \rho\omega/k$, $Z^\star$ depends on k in a complicated way. If the attenuation length is larger than the sample thickness, *i.e.* $k''d \ll 1$, eq. (3) can be simplified into

$$\frac{Z_0}{Z^\star} = -\mathrm{i}\frac{Z_0}{\omega\rho}(k' + \mathrm{i}k'')\frac{\tan(k'd) + \mathrm{i}k''d}{1 - \mathrm{i}k''d\tan(k'd)}\,. \tag{4}$$

An analysis of eq. (4) shows that the real part of the admittance reaches a maximum for $k'd = \pi/2$ (modulo π). This is confirmed by our experiments, as shown in fig. 3 which reports the dimensionless input admittance measured on a liquid foam sample as a function of frequency. The real part of the admittance indeed shows many peaks.

[1] The impedance of air is $Z_0 = \rho_0 c_0$, where ρ_0 is the density of air and c_0 the speed of sound in air; $Z_0 = 413\,\mathrm{N\,s/m^3}$ at normal conditions (temperature of 20 °C and atmospheric pressure of 101 kPa).

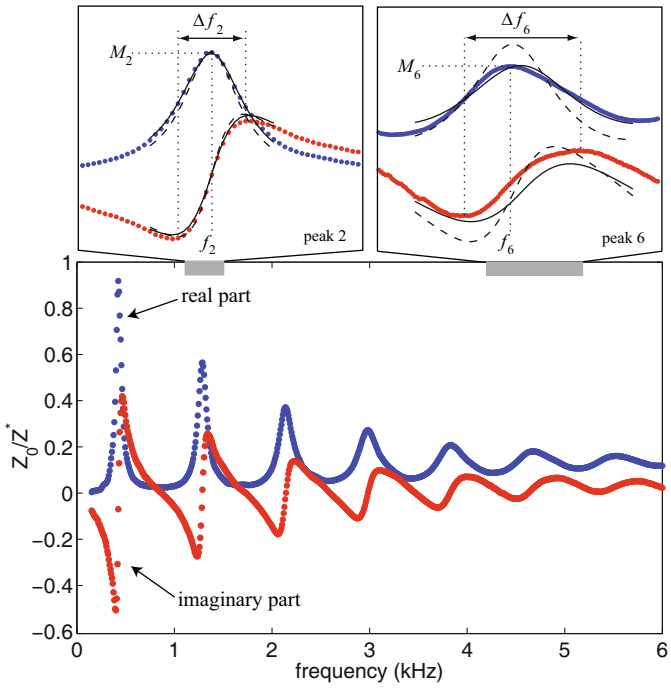

Fig. 3. Dimensionless input admittance measured as a function of the frequency; here for sample SDS 10% A, with thickness $d = 1.93 \pm 0.05$ cm. Insets: close-ups of the second and sixth peaks, showing result of the local fitting. Equation (3) is plotted for two cases: with the parameters given by eqs. (5) (dashed lines) and with the ones given by the least square fit (solid lines).

As the peaks are quite narrow, it seems reasonable to assume that k and ρ do not vary significantly with frequency within a peak. Then one can calculate that, as long as eq. (4) holds, the velocity $v = \omega/k'$, attenuation $\alpha = k''$ and mass density ρ of the sample can be determined by three features of peak n: frequency f_n and amplitude M_n of its maximum, and width Δf_n. For peak number n, one then has (see appendix E)

$$v = \frac{4df_n}{1+2(n-1)}\,, \tag{5a}$$

$$\rho = \frac{Z_0}{\pi d \Delta f_n M_n}\,, \tag{5b}$$

$$\alpha = [1+2(n-1)]\pi\frac{\Delta f_n}{4df_n}\,. \tag{5c}$$

As an example, for the second peak of fig. 3, one can measure $f_2 = 1.29$ kHz, $\Delta f_2 = 0.10$ kHz and $M_2 = 0.565$, which leads to $\rho = 119\,\mathrm{kg/m^3}$, $v = 33$ m/s, $\alpha = 9\,\mathrm{m^{-1}}$. When eq. (3) is plotted with these values (see top left inset in fig. 3, dashed lines), a good agreement is found with the experimental data. However, as the attenuation increases with frequency, the $k''d \ll 1$ approximation becomes less accurate at higher frequencies. For example, for the sixth peak, when eq. (3) is plotted with the values given by eqs. (5), the agreement is not satisfactory. A better agreement is obtained when a least square fit is performed, using the values of eqs. (5) as first guesses (see solid lines in the insets of fig. 3). Note that the fitting is done only on the real part of the admittance, because the imaginary part is sensitive to the exact position of the surface of the sample (see appendix D).

From the $Z_0/Z^\star$ *vs.* f curve, the peaks were fitted to determine ρ, v and α as functions of frequency. The number of frequency points accessible depended on the number of peaks one could analyze. For sample SDS 10% A (fig. 3), seven peaks could be analyzed, given access to measurements from 0.5 to 5.5 kHz.

4 Results

4.1 Velocity and density

It is important to note that, throughout this article, we call density (noted ρ) the *effective* density of the foam, *i.e.* the one measured acoustically which we then compare to the density measured by non-acoustic means, refered to as the "liquid fraction" in order to make the difference. Figures 4a and b show the density and velocity found for the eight different liquid foam samples presented in table 1. For each liquid fraction, very similar results are found for samples A and B, indicating that Φ is the main parameter governing v and ρ. As expected for liquid foams, very low sound velocities are found. Furthermore, the measured densities are very close to the average densities of the sample (see inset of fig. 4d).

For the six SDS foams, the velocity is found to be constant with frequency. On the other hand, the densities seem to decrease with frequency, the slope being more pronounced for humid foams. Even though effective densities decreasing with frequency have been reported in porous materials [3], it is hard to believe this effect to be physical, especially because this should also give a frequency dependence for the velocity. An explanation based on the effect of the density gradient in the foam is investigated in appendix C. Another plausible explanation invokes the existence of guided modes in the tube. Indeed, the condition for only plane waves to propagate in the tube is $\lambda \geq 2D$, where λ is the acoustic wavelength and D the diameter of the tube. The impedance tube is specifically designed for this condition to be fullfilled in air. But in the sample, given the very low velocities in liquid foams, the wavelength can become smaller than the diameter (for $v = 25$ m/s, $\lambda = 2.5$ cm at 1 kHz, to be compared to $D = 2.9$ cm for the tube we used). It is therefore possible that other modes than plane waves are excited in the foam sample, which would lead to a lower reflection coefficient. According to eqs. (2) and (5b), the amplitude of the admittance peak is larger when the reflection is smaller, thus leading to a lower measured density. This explanation is consistent with the experimental observation because one then expects the decrease of the estimated density to be more pronounced for high frequencies and low velocities. Note that, within this scenario, the velocity and attenuation measurements are expected to be insensitive to this effect, because they depend on the positions and widths of the peaks, not on their amplitudes.

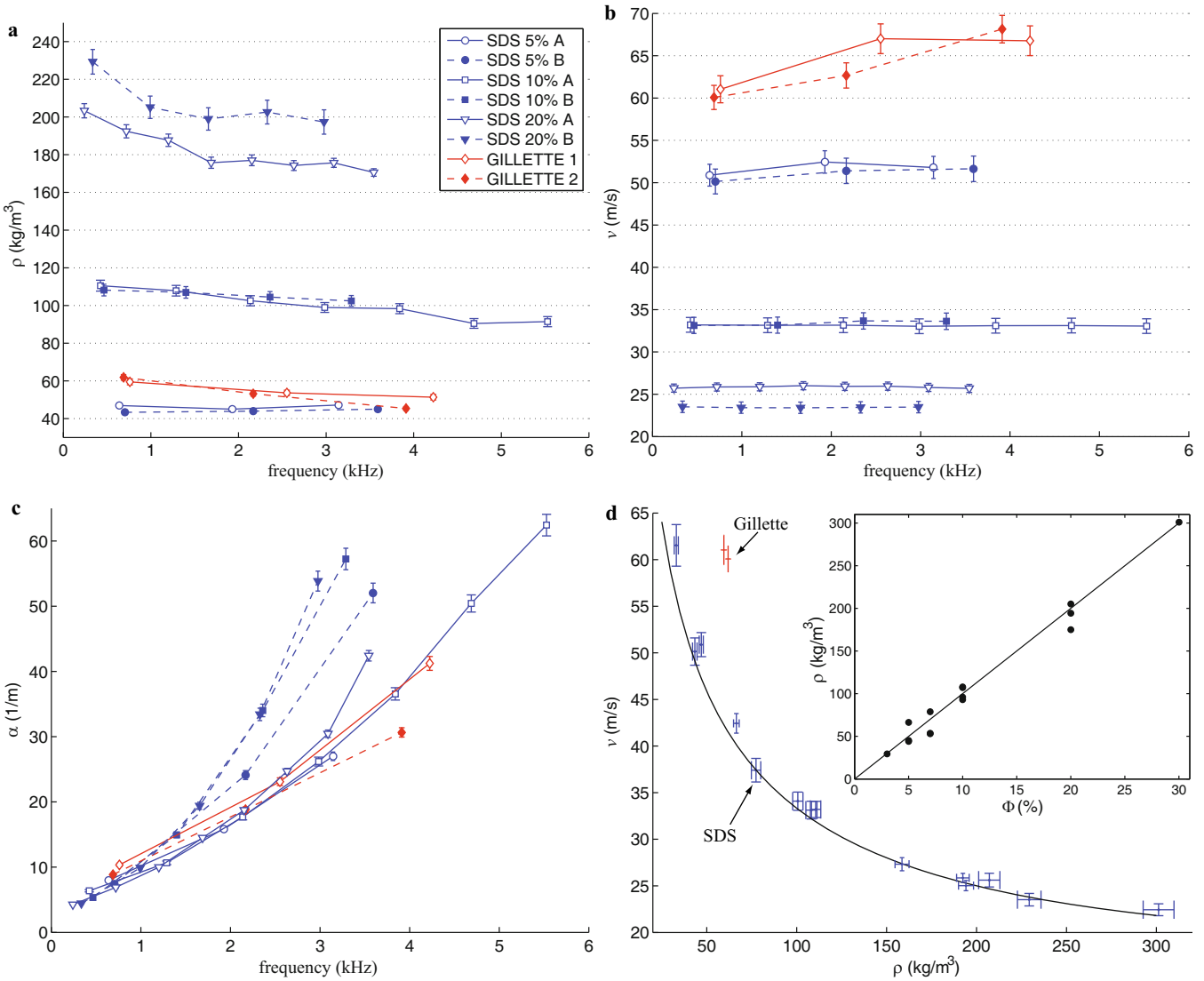

Fig. 4. Measured density (a), velocity (b) and attenuation (c) as functions of the frequency for the 8 selected foams (see table 1). (d) Sound velocity as a function of density for all the samples. Note that the values of ρ reported here correspond to the *acoustical* measurements. The inset shows that ρ depends on Φ with the expected law (continuous line is $\Phi\rho_\ell$).

For the two Gillette samples, the situation is different because as the measured density is found to decrease by about 20% when going from 1 to 4 kHz, the measured velocity increases by 10%. Thus a frequency-dependent effective density might be physical for these samples.

As shown in fig. 4d, an excellent agreement is found between Wood's prediction and the measured velocity as a function of the measured density[2] in SDS samples with liquid fractions ranging from 3 to 30%. The inset of fig. 4d shows the measured density as a function of the liquid fraction of the foam, which we know from the preparation protocol. As one can see, both values are in good agreement.

In Gillette samples, the velocity is significantly higher than Wood prediction. This anormally high sound velocity in Gillette was already reported [9,14,11]. The novelty of our result is that we have access to the structure of the foam since we know the bubble size distribution. We hence know that SDS 5% A and Gillette 2 samples are very similar in terms of bubble sizes (see fig. 2) and liquid fractions. It therefore confirms Mujica and Fauve's hypothesis [9] that the origin of the high sound velocity in Gillette is to be looked for in its physico-chemical composition.

4.2 Attenuation

In contrast to velocity and density measurements, attenuation is found to be very dispersive and with no clear dependence on the liquid fraction (see fig. 4c). The attenuation is of the same order of magnitude in all the samples,

[2] Equation (1) was taken for Wood's law, with $\Phi = \rho/\rho_\ell$. Effective densities ρ were taken as measured on the first peak because both interpretations for the frequency dependence of ρ give more credit to the low frequency value.

including Gillette samples. However, SDS B-samples seem to attenuate more than A-samples, suggesting that either the gas content or the bubble size distribution have an effect on the acoustic attenuation.

The measured attenuations can be compared to predictions of two models: Wood and Goldfarb-Shreiber-Vafina (GSV) model. A more detailed discussion of these models is given in appendix F. It turns out that Wood's model, for which only thermal losses are significant, under-estimates the attenuation, whereas GSV over-estimates it (see fig. 7 in appendix F).

5 Conclusions

Using foam samples with known physico-chemical properties and bubble size distributions, we have shown here that a vertically mounted, commercial impedance tube can be used to measure the velocity v and absorption α of acoustic waves in a 0.5–6 kHz range in liquid foams. Moreover from the low-frequency measurements of the effective density ρ, one can estimate the liquid volume fraction Φ of the foam, which gives an alternative method to weighting or to conductivity measurement. Acoustic velocity in SDS foams was found to be independent of the bubbles size and in excellent agreement with Wood's predicition. On the other hand, in foams with the same structure but different composition (Gillette) sound propagates at a significantly higher velocity, suggesting that either bulk or surface elasticity may play a role in the acoustic properties of the foam. More systematic investigations are needed to elucidate this point, as well as the exact mechanisms involved in the attenuation.

In principle, the technique is fast enough to provide time-resolved measurements, hence giving acces to the time evolution of the acoustic properties, which could be related to the evolution of the structure of the foams (drainage, coarsening, film rupture). Impedance tube thus appears as a promissing new tool for investigating acoustic properties of liquid foams, which may help to shed light on the high-frequency mechanics of interfaces.

Support for the French Agence Nationale de la Recherche (project SAMOUSSE, ANR-11-BS09-001) is gratefully acknowledged. The authors thank Imane Boucenna and Cyprien Gay for fruitful discussions.

Appendix A. Image analysis

The bubble size distribution is determined using images of a monolayer of bubbles, which we create by depositing a small drop of foam on a pool of the foaming solution. We image these monolayers in front of a large diffusive light source using a digital camera. For each foam sample, several images are taken to obtain representative statistics.

In order to obtain the bubble size distributions, we use the open-source software *ImageJ*[3] in combination with a special protocol. To illustrate this protocol we use the sample Gillette 2 as an example. In a first step, a threshold and an inversion is applied to the bubble raft images (see fig. 5a). As a result, all bubbles contain a black, circular area. The relationship between the size of this black disk and the real bubble size is fixed by elementary optics of light being transmitted through the bubbles. In particular, one finds that both quantities are linearly related (fig. 5b) with the pre-factor depending on the particular set-up used. After doing a calibration measurement to obtain this prefactor, it is used for all foams imaged with the same set-up to calculate the real bubble size from the size of the disk.

The advantage of the black disks is that they can be found easily by the *ImageJ* program in an automatic manner using the "analyse particles" routine in combination with the circularity of the detected object. The size distribution of the disks is then related to the size distribution of the bubbles via the pre-factor established in fig. 5b. From this we obtain histograms as the one shown in fig. 2.

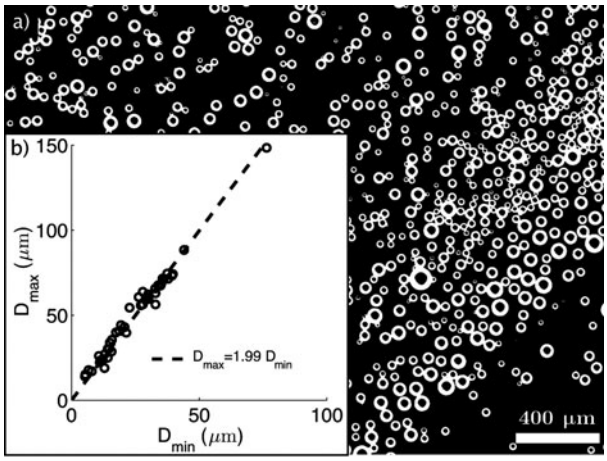

Fig. 5. (a) Images of the monolayer (here for sample Gillette 2) are thresholded and inversed. (b) The real diameter of each bubble is found to scale linearly with the diameter of the black disk inside the bubble.

Appendix B. Comparison with previous experimental results

Table 2 proposes a summary of different acoustical measurements available on liquid foams. For the sake of comparison, we focus here on foams whose liquid volume fraction is of the order of 5%, a category that includes shaving foams. Apart from the impedance tube technique described in this article, three different setups have been used:

– *Shock tube.* A thin membrane separates the foam from a high-pressure chamber. When the membrane is punctured, an acoustic wave is emitted and its propagation is recorded by a serie of six microphones, giving thus access to the velocity and attenuation. The typical frequency content of the propagating pulse is 0.1–1 kHz.

[3] `http://rsbweb.nih.gov/ij/`

Table 2. Comparison of the present study with previous acoustical measurements on liquid foams.

Authors	Setup	Foam	Phase velocity	Attenuation	Frequency	Average radius
Orenbackh and Shushkov [5]	Shock tube	$\Phi = 5\%$, air + water + unknown surfactant	$v = 50\,\mathrm{m/s}$	$\alpha = 3.5\,\mathrm{m}^{-1}$ $\alpha\lambda = 1.7$	$\sim 0.1\,\mathrm{kHz}$	$\sim 100\,\mu\mathrm{m}$
Mujica and Fauve [9]	Transmission with moving receiver	$\Phi = 8\%$, Gillette (regular)	$v = 65\,\mathrm{m/s}$	$\alpha = 115\,\mathrm{m}^{-1}$ $\alpha\lambda = 0.20$	37 kHz	
Shreiber *et al.* [6]	Shock tube	$\Phi = 5\%$, air + expandol solution	$v = 48\,\mathrm{m/s}$	$\alpha = 5.5\,\mathrm{m}^{-1}$ $\alpha\lambda = 2.6$	$\sim 0.1\,\mathrm{kHz}$	100–200 μm
Daugelaite [14]	Transmission with fixed receiver	$\Phi = 7\%$, Gillette (sensitive)	$v = 60\,\mathrm{m/s}$	$\alpha = 200\,\mathrm{m}^{-1}$ $\alpha\lambda = 0.32$	37 kHz	15 μm
Ben Salem *et al.* [11]	Transmission with fixed receiver	$\Phi = 7\%$, Gillette	$v = 60\,\mathrm{m/s}$		40 kHz	15 μm
Present paper	Impedance tube	$\Phi = 7\%$, Gillette (sensitive)	$v = 60\,\mathrm{m/s}$	$\alpha = 9\,\mathrm{m}^{-1}$ $\alpha\lambda = 0.77$	0.7 kHz	22 μm
		$\Phi = 5\%$, air+C_2F_6 in SDS + xanthane	$v = 50\,\mathrm{m/s}$	$\alpha = 8\,\mathrm{m}^{-1}$ $\alpha\lambda = 0.67$	0.6 kHz	38 μm

– *Transmission with moving receiver.* A transducer placed at the bottom of the foam sends an acoustic signal recorded by a receiver, whose distance to the emitter can be varied. Acoustic velocity and attenuation are deduced from the measurements of the time of flight and amplitude as functions of the distance.

– *Transmission with fixed receiver.* The setup is similar to the previous one but instead of changing the emitter-receiver distance *in* the foam, different acquisitions with equivalent samples of different thicknesses are performed. It requires a good reproductibility of the foam samples.

The four studies on Gillette foams found very similar velocities of sound, significantly higher than for the other types of foams, in which Wood's law is verified. As attenuation is strongly frequency dependent, comparison between the different studies is more delicate. The attenuation per wavelength $\alpha\lambda = \alpha v/f$ (where f is the frequency) seems to be a decreasing function of the frequency.

By measuring the attenuation on a coarsening Gillette foam, Mujica and Fauve observed that $\alpha\lambda \sim R^2 f$. It seems that this law does not extend to low frequencies: our measurements with Gillette at 0.7 kHz give indeed an attenuation per wavelength twice larger than in Daugelaite's experiment at 37 kHz, whereas the $R^2 f$ law would predict a ratio 1/25.

Appendix C. Liquid fraction gradient and its effect on the acoustic measurements

Due to gravity, a gradient of liquid fraction is expected to be present within the foam. At equilibrium, it has been shown that the liquid fraction profile can be accurately predicted if the capilary length, the total liquid fraction in the foam, and the Sauter mean radius of the bubbles

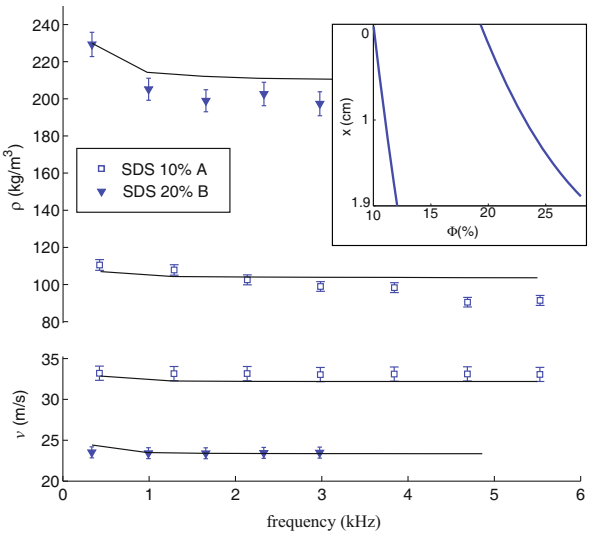

Fig. 6. For two SDS samples, the experimental values found for ρ and v are compared to what is expected when the density profile is accounted for (inset).

can be determined [19]. Figure 6 reports the calculated profiles (see inset) for two of our SDS foams: SDS 10% A ($\Phi = 11\%$, $R_{32} = 36\,\mu$m and $d = 1.9\,$cm) and SDS 20% B ($\Phi = 23\%$, $R_{32} = 46\,\mu$m and $d = 1.8\,$cm). For the dryier foam, the liquid fraction is found to be almost homogeneous (from 12% to 10%, from bottom to top). However, for the wetter sample, a significant gradient exists (28 to 19%).

From these profiles, we can calculate the input admittance of the sample by modelling it as a multiple layer medium [20], with air on top ($x = 0$) and an infinitely rigid backplate at the bottom ($x = d$). Following the same analysis procedure as for the experimental data, we can

then extract the velocity and density one would measure from this calculated admittance. Figure 6 shows the comparison between these simulated results and the actual experimental measurements. It appears that the existence of a liquid fraction gradient does lead to an acoustically measured density that decreases with frequency. However, the dependence is not as strong as in the experiments. Furthermore, the calculated density gradient is probably over-estimated because it corresponds to an equilibrium state, whereas the measurement is done quickly after the filling of the tube. Density gradient might play a role in the acoustic measurements of ρ but further experimental studies will be necessary to investigate this point.

Appendix D. Effect of the position of the air-sample interface

If the air-sample interface is not at $x = 0$ but at $x = x_0$ (see fig. 1c), the new relationship between the measured reflection and the impedance is

$$\frac{Z_0}{Z} = \frac{\mathrm{i}}{\tan k(d - x_0)} \times \frac{1 - \mathcal{R}\mathrm{e}^{-2\mathrm{i}k_0 x_0}}{1 + \mathcal{R}\mathrm{e}^{-2\mathrm{i}k_0 x_0}}\,. \tag{D.1}$$

It has two consequences on the analysis described in sect. 3:

- The sample thickness should be taken as $d - x_0$ rather than d. This is actually the main source of uncertainty when we measure v, α and ρ; error bars in fig. 4 were calculated from the ± 0.5 mm accuracy of our thickness measurement.
- There is an additional $2k_0x_0$ phase shift in the reflection coefficient, because the length of propagation in air is larger (or shorter, if $x_0 < 0$). As x_0 is usually small compared to the wavelength, the phase shift is small and only affects the imaginary part $Z_0/Z^\star$. This is why the analysis procedure we propose relies on the real part of the admittance.

This sensitivity to the air-sample interface position is a limitation of the technique for time resolved measurements. Indeed, as the liquid foam is ageing, d generally increases (due to gas diffusion), which has a strong effect on the acoustic measurements, thus masking effects that could be due to finer structure changes. An improvement would be to add a membrane at $x = 0$ that would be stiff enough to block the foam, but thin enough to be acoustically transparent.

Appendix E. Derivation of eqs. (5)

This appendix gives details upon the analysis of eq. (4) to find the positions and amplitudes of the peaks. Let us recall that when condition $k''d \ll 1$ is satisfied, eq. (3) reduces to

$$\frac{Z_0}{Z^\star} = -\mathrm{i}\frac{Z_0}{\omega\rho}(k' + \mathrm{i}k'')\frac{\tan(k'd) + \mathrm{i}k''d}{1 - \mathrm{i}k''d\tan(k'd)}\,. \tag{E.1}$$

A maximum of the real part of this formula is reached when $k'd = \pi/2 + n\pi$ ($\tan k'd \to \pm\infty$). The velocity can thus be calculated by the frequency of this maximum (eq. (5a)). This maximum $M_n = Z_0k'/(\omega\rho k''d)$ depends on the velocity (k'), the attenuation (k''), and the density (ρ). Providing that the attenuation is determined, M_n can thus give access to the density (eq. (5b)).

To determine the attenuation, one can analyse eq. (E.1) close to the peak: $k'd = \pi/2 + n\pi + \epsilon$, which gives $\tan k'd \sim -1/\epsilon$. A minimum of the imaginary part of the admittance is found for $\epsilon = -k''d$, followed by a maximum for $\epsilon = +k''d$. The distance between these two extrema thus gives access to the attenuation (eq. (5c)).

Note that the density is supposed to be real in our analysis. This is an approximation: it has been rigorously deduced using homogenisation theory that the effective acoustic density in a visco-thermal fluid is a *complex*, frequency-dependent quantity [21,22,3]. However, we expect the imaginary part of ρ to be small compared to its real part, bringing only a negligible correction to our results.

Appendix F. Models

We briefly present two theoretical models whose predictions can be compared to our experimental results. The first one is a generic model for acoustics in two-phase systems (Wood), whereas the other one was specifically developped for liquid foams by Goldfarb, Shreiber and Vafina (GSV).

Appendix F.1. Wood model

Wood's law [7] (also known as the mixture law) is based on the effective density ρ_{eff} and effective compressibility χ_{eff} of the medium, from which the effective wave number k can be calculated: $(k/\omega)^2 = \rho_{\mathrm{eff}}\chi_{\mathrm{eff}}$, where ω is the angular frequency. The effective density is given by

$$\rho_{\mathrm{eff}} = \Phi\rho_\ell + (1 - \Phi)\rho_g \simeq \Phi\rho_\ell, \tag{F.1}$$

where ρ_ℓ and ρ_g are the mass density of the liquid and the gas, respectively. For the compressibility, one can consider a large volume V that contains N bubbles of radius R

$$V = N\frac{4}{3}\pi R^3 + V_\ell, \tag{F.2}$$

where V_ℓ is the volume of the liquid. Then, by definition of the effective compressilbity ($\chi_{\mathrm{eff}} = -(1/V)\partial V/\partial P$), one obtains

$$\chi_{\mathrm{eff}} = -3(1 - \Phi)\frac{1}{R}\frac{\partial R}{\partial P} + \Phi\chi_\ell. \tag{F.3}$$

One then needs to determine how the bubbles react when they are submitted to a pressure change. To a first approximation only the compressibility of the gas matters, which leads to an equation similar to eq. (F.1). As bubble dynamics have been extensively studied, a better solution can be easily obtained, for instance by taking the

linearized Rayleigh-Plesset equation [23]. It leads to

$$\left(\frac{k}{\omega}\right)^2 = \frac{\rho_\ell \Phi(1-\Phi)}{\kappa P_0 + \frac{2\sigma}{R_0}(\kappa - 1/3) - \frac{\omega^2 \rho_\ell R_0^2}{3} - \frac{4\mathrm{i}\eta\omega}{3}}, \quad \text{(F.4)}$$

where the density of the gas and the compressiblity of the liquid have been neglected. In eq. (F.4), σ is the surface tension, P_0 the ambient pressure, η the viscosity of the liquid, R_0 the equilibrium radius of the bubbles, and κ the complex polytropic exponent for the thermal transformations of the gas, given by [24]

$$\kappa = \frac{\gamma}{1 - 3(\gamma-1)\frac{1-[(1+\mathrm{i})R_0/\ell_{\mathrm{th}}]\coth[(1+\mathrm{i})R_0/\ell_{\mathrm{th}}]}{[(1+\mathrm{i})R_0/\ell_{\mathrm{th}}]^2}}, \quad \text{(F.5)}$$

with γ the ratio of the specific heat for the gas, and $\ell_{\mathrm{th}} = \sqrt{2D_{\mathrm{th}}/\omega}$ the thermal length (D_{th} is the gas thermal diffusion coefficient).

For the range of bubble radii and frequencies investigated in our experiment, surface tension and inertia terms can be neglected in eq. (F.4)[4]. Thus, the real part of κ being very close to 1, equation (1) is recovered.

Equation (F.4) accounts for two sources of dissipation of the acoustic energy: thermal losses (imaginary part of κ) and viscous losses (term with viscosity η). As pointed out by Mujica and Fauve [9], thermal losses dominate over the viscous ones if η is close to the viscosity of water. Note that this extended version of Wood law gives the same dispersion relation as Waterman and Truell [25].

Appendix F.2. GSV model

In the model proposed by Golfarb and coworkers [26,27] the particular structure of the foam is taken into account. From the thermal point of view, it consists in acknowledging the smallness of the volumes of water between the air bubbles, which makes arguable the status of infinite thermal source given to the liquid phase in Wood's model. In practice, this effect brings only small changes to the dispersion relation. On the other hand, the structure of the foam modifies significantly the predicted viscous losses. Indeed, instead of the bulk viscosity of the liquid, one needs to consider the resistance to liquid flows that exists in the network of liquid channels. In analogy to flows in porous media, one can use the Darcy law and introduce a permeability K. A good approximation to GSV prediction can be recovered by changing η into $\eta(1 + \Phi R_0^2/4K)$ in eq. (F.4). GSV model takes $K = 3.5 \times 10^{-3} R_0^2 \Phi^2$ to relate the permeability to the structure of the foam, a relation very close to the channel-dominated law which is known to give a good order of magnitude for liquid foams [28][5].

[4] For the following typical values: $\sigma = 40\,\mathrm{mN/m}$, $R_0 = 20\,\mu\mathrm{m}$, and $\omega/2\pi = 1\,\mathrm{kHz}$, $2\sigma/R_0 \simeq 3\times10^3\,\mathrm{Pa}$ and $\omega^2\rho_\ell R_0^2/3 \simeq 5\,\mathrm{Pa}$, both negligible compared to $\mathrm{Re}(\kappa)P_0 \simeq 10^5\,\mathrm{Pa}$.

[5] We corrected what we believe to be an error in eq. (16) of ref. [27], in which an extra Φ appears in factor of η, and the permeability law scales as Φ^3.

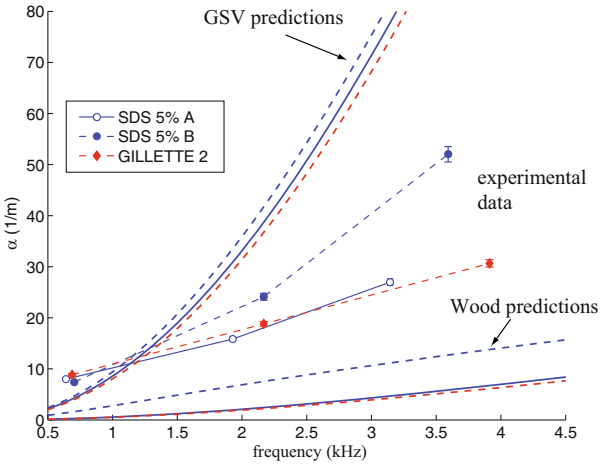

Fig. 7. Comparison between the measured and predicted attenuation for three samples.

The effective viscosity experienced by a bubble oscillating in a liquid foam would thus be much higher than the simple viscosity of the liquid phase considered in Wood's model (η is multiplied be a factor of about $70/\Phi$).

Appendix F.3. Comparison with experiments

For comparison with experimental data (fig. 7), one needs to take the polydispersity into account, and determine the thermal and mechanical parameters of the media. For Wood's model, polydispersity is taken into account by letting N depend on R in eq. (F.2): $N(R)$ being given by the measured histogram. In the case of GSV model, the mean radius was considered (see table 1). For both models, the following thermal parameters were estimated [29]: $\gamma = 1.1$, $D_{\mathrm{th}} = 8 \times 10^{-6}\,\mathrm{m^2/s}$ for air saturated with C_6F_{14} (SDS A-samples), $\gamma = 1.2$, $D_{\mathrm{th}} = 12 \times 10^{-6}\,\mathrm{m^2/s}$ for air partially saturated with C_6F_{14} (SDS B-samples), and $\gamma = 1.2$, $D_{\mathrm{th}} = 5 \times 10^{-6}\,\mathrm{m^2/s}$ for Gillette samples. The viscosity of water was taken ($\eta = 10^{-3}\,\mathrm{Pa\,s}$) for both SDS and Gillette samples. This is a good approximation for Gillette [30]. On the other hand, since it contains xanthane, the SDS foaming solution we used is probably more viscous. Measurements in a rheometer showed that its viscosity was decreasing with frequency (as expected for a shear-thinning fluid), with a value of $10^{-2}\,\mathrm{Pa\,s}$ at 10 Hz, for a strain ranging from 0.1 to 10%. As the acoustic frequencies we used are two order of magnitude higher, taking the viscosity of water seems a reasonable order of magnitude.

For the sake of clarity, we show comparison for three samples only, in fig. 7: the two SDS at $\Phi = 5\%$ and one of the Gillette samples. Wood's model, for which only thermal losses are significant, predicts attenuation that are lower than what is measured, but the relative attenuation from one sample to the other is well predicted: SDS B attenuates more than the other two. The same observations can be made for the five other samples. Contrary to Wood's model, GSV model estimates that viscous losses

are significant, due to the liquid flowing through a network of narrow channels. As shown in fig. 7, it seems to over-estimate the attenuation. Our experimental results thus indicate that a precise model for the attenuation of sound in liquid foams is still to be found.

Note that in the impedance tube, an additional source of attenuation can arise, due to dissipation on the wall of the tube. This attenuation is given by Kirchhoff law [13] and it is proportional to the diffusive length for thermal and/or viscous exchanges. As this length is inversely proportional to the square root of the frequency, Kirchhoff attenuation is stronger at low frequency. It could explain the fact that the experimental attenuation does not seem to reach zero at zero frequency (see fig. 7).

References

1. D. Weaire, S. Hutzler, *The Physics of Foams* (Clarendon Press, Oxford, 1999).
2. I. Cantat, S. Cohen-Addad, F. Elias, F. Graner, R. Hohler, O. Pitois, A. Saint-Jalmes, *Les mousses : structure et dynamique* (Belin, 2010).
3. J.F. Allard, N. Atalla, *Propagation of Sound in Porous Media* (Wiley, 2009).
4. A.S. Dukhin, P.J. Goetz, Adv. Colloid Interface Sci. **92**, 73 (2001).
5. Z.M. Orenbakh, G.A. Shushkov, Acoust. Phys. **39**, 63 (1993).
6. I. Shreiber, G. Ben-Dor, A. Britan, V. Feklistov, Shock Waves **15**, 199 (2006).
7. A.B. Wood, *A Textbook of sound* (Bell, London, 1932).
8. V.V Zamashchikov, N.A. Kakutkina, Sov. Phys. Acoust. **37**, 248 (1991).
9. N. Mujica, S. Fauve, Phys. Rev. E **66**, 021404 (2002).
10. J. Ding, F.W. Tsaur, A. Lips, A. Akay, Phys. Rev. E **75**, 041601 (2007).
11. I. Ben Salem, R.-M. Guillermic, C. Sample, V. Leroy, A. Saint-Jalmes, B. Dollet, Soft Matter **9**, 1194 (2013).
12. J. Pierre, F. Elias, V Leroy, Ultrasonics **53**, 622 (2013).
13. T.D. Rossing, *Springer Handbook of Acoustics* (Springer Verlag, 2007).
14. D. Daugelaite, PhD thesis, University of Manitoba (2011).
15. K.C. Symers, Food Chem. **6**, 63 (1980).
16. J. Sauter, VDI-Forschungsheft, 279 (1926).
17. Determination of sound absorption coefficient and impedance in impedance tubes, ISO 10534-2, International Organization for Standardization, Geneva, Switzerland (2002).
18. A.F Seybert, D.F. Ross, J. Acoust. Soc. Am. **61**, 1362 (1977).
19. A. Maestro, W. Drenckhan, E. Rio, R. Hohler, Soft Matter **9**, 2531 (2013).
20. L.M. Brekhovskikh, *Waves in Layered Media* (Academic, New York, 1960).
21. J.L. Auriault, C. Boutin, C. Geindreau, *Homogenization of coupled Phenomena in Heterogenous Media* (John Wiley and Sons, 2009).
22. J.L. Auriault, L. Borne, R. Chambon, J. Acoust. Soc. Am. **77**, 1641 (1985).
23. A. Prosperetti, J. Acoust. Soc. Am. **56**, 878 (1974).
24. A. Prosperetti, L.A. Crum, K.W. Commander, J. Acoust. Soc. Am. **83**, 502 (1988).
25. P.C. Waterman, R. Truell, J. Math. Phys. **2**, 512 (1961).
26. I.I Goldfarb, I.R. Schreiber, F.I. Vafina, J. Acoust. Soc. Am. **92**, 2756 (1992).
27. I.I Goldfarb, Z. Orenbakh, I.R. Schreiber, F.I. Vafina, Shock Waves **7**, 77 (1997).
28. E. Lorenceau, N. Louvet, F. Rouyer, O. Pitois, Eur. Phys. J. E **28**, 293 (2009).
29. A.L. Lindsay, L.A. Bromley, Indust. Engin. Chem. **42**, 1508 (1950).
30. A.D. Godal, D.J. Durian, J. Colloids Interface Sci. **213**, 169 (1999).